School of Natural Sciences and Mathematics
William B. Hanson Center for Space Sciences

Motions of ihe Convection Reversal Boundary and Local Plasma in the High-Latitude Ionosphere

UT Dallas Author(s):

Yun-Ju Chen
Roderick A. Heelis

Citation:

Chen, Yun-Ju, and Roderick A. Heelis. 2018. "Motions of the Convection Reversal Boundary and Local Plasma in the High-Latitude Ionosphere." Journal of Geophysical Research: Space Physics 123(4): 2953-2963, doi: 10.1002/2017JA024934

Journal of Geophysical Research: Space Physics

RESEARCH ARTICLE
10.1002/2017JA024934

Motions of the Convection Reversal Boundary and Local Plasma in the High-Latitude Ionosphere

Yun-Ju Chen[1] and **Roderick A. Heelis**[1]

[1]William B. Hanson Center for Space Sciences, University of Texas at Dallas, Richardson, TX, USA

Key Points:
- Plasma and CRB motion are consistent with adiaroic behavior if jitter motion over a few minutes is superimposed on a monotonic CRB motion
- Viscous-like interaction may contribute to the differences in plasma and CRB motion at an adiaroic boundary

Correspondence to:
Y.-J. Chen,
yxc126130@utdallas.edu

Citation:
Chen, Y.-J., & Heelis, R. A. (2018). Motions of the convection reversal boundary and local plasma in the high-latitude ionosphere. *Journal of Geophysical Research: Space Physics*, *123*, 2953–2963. https://doi.org/10.1002/2017JA024934

Received 30 OCT 2017
Accepted 9 MAR 2018
Accepted article online 23 MAR 2018
Published online 6 APR 2018

Abstract We present results from a systematic study of multisatellite samplings from the Defense Meteorological Satellite Program F13, F15, F16, F17, and F18 satellites over the period from 2007 to 2015 that describe the motion of the convection reversal boundary (CRB) and the local plasma flow across it. Focusing on the cases with continuous poleward and equatorward CRB motion sampled by three consecutive satellites within 50 min, 45% of the time the CRB motion may deviate from the local plasma motion near dawn and dusk where the reconnection process is unlikely to be present. Differences in the inferred CRB motion and the local plasma motion may arise from apparent motion induced by the local time displacement of consecutive samples across the CRB that is tilted with respect to a line of constant latitude. The presence of a viscous-like interaction across the CRB can also contribute to the difference in the CRB and plasma motion. Accounting for these processes, the CRB motion and the motion of the plasma at the CRB are consistent only if a back and forth motion over a timescale of a few minutes is superimposed on a monotonic migration of the CRB over longer time periods.

1. Introduction

Both reconnection processes (Dungey, 1961) and viscous-like interaction (Axford & Hines, 1961) are associated with plasma convection in the high-latitude ionosphere, which displays a two-cell pattern during periods of southward interplanetary magnetic field (IMF). The electric potential distribution across the polar region associated with reconnection or viscous-like interaction has been studied extensively (Axford, 1964; Boyle et al., 1997; Drake et al., 2009; Lockwood et al., 2009; Mozer, 1984; Sonnerup et al., 2001; Sundberg et al., 2008). It is found that during periods of southward IMF viscous-like interaction contributes about 10% of the total potential difference (~100 kV) across the magnetopause, suggesting that the overall configuration of the convection pattern is dominated by the reconnection process (Chen et al., 2016; Sundberg et al., 2008).

Several statistical studies and models of the convection pattern have been conducted utilizing satellite and radar observations (Cousins & Shepherd, 2010; Rich & Hairston, 1994; Ruohoniemi & Greenwald, 1996; Weimer, 2001, 2005) that give us a large-scale view of the convection pattern and its response to different states in the solar wind. Other studies have been dedicated to the timescale for response of the convection pattern to a sudden change in the IMF B_z component (Fiori et al., 2012, and references therein). The timescales ranging from 10 to 30 min are consistent with those over which the convection pattern is initially excited on the dayside and propagates toward the nightside to accomplish a reconfiguration of the whole flow pattern (Cowley & Lockwood, 1992; Fiori et al., 2012; Hairston & Heelis, 1995; Nishitani et al., 2002; Ridley et al., 1998).

The expanding/contracting polar cap model (Cowley & Lockwood, 1992; Siscoe & Huang, 1985) specifies that the time evolution of the convection pattern is determined by the time evolution of the reconnection rates at the dayside and nightside polar cap boundaries. When the dayside reconnection rate is larger than the nightside reconnection rate, the polar cap boundary (PCB) expands. When the dayside reconnection rate is smaller than the nightside reconnection rate, the PCB contracts. The evolution of the shape of the PCB during such expansions and contractions is poorly specified but likely depends on the evolution of the drivers on the dayside and the nightside (Cowley & Lockwood, 1992; Lockwood & Morley, 2004; Morley & Lockwood, 2006). During the transition from one quasi steady state to another, the boundary may not appear nominally as a circle with a uniform radius. Recent statistical analyses of the location of the convection reversal boundary have shown evidence for such a propagating reconfiguration as well as a dependency on the IMF orientation (Bristow & Spaleta, 2013; Chen et al., 2015; Koustov & Fiori, 2016).

When the dayside and nightside reconnection sites are isolated regions, the segments of the PCB between these two sites around dawn and dusk are sometimes referred to as adiaroic boundaries, which move with

the local plasma with no plasma flow across them (Siscoe & Huang, 1985). In the absence of flows due to a viscous-like interaction, the CRB and the PCB are collocated and any observed plasma flow across these boundary segments then represent expansions and contractions of the boundaries in response to changes in dayside and nightside reconnection rates. If the CRB is stationary, then the CRB will be a sheer flow boundary with no plasma flow across it. When a viscous-like interaction is present, then the CRB lies just equatorward of the PCB and the observed flows across the CRB are consistent of those produced by the viscous-like interaction and the motions of the CRB.

The PCB is poorly defined by the convective flows near a dayside reconnection site (Heelis, 1984; Moses et al., 1988) since local excursions of the boundary caused by the addition of open magnetic flux will occur. Substantial movements of the PCB and the flow reversal boundary have been reported by earlier studies to be up to 5° in latitude within 15 min in universal time depending on the local time sector (Brittnacher et al., 1999; Ridley & Clauer, 1996). Further statistical investigations of substorm events also show approximately the same spatial and temporal variability across midnight (Gjerloev et al., 2008; Laundal et al., 2010).

This study is pursued to examine the extent to which the adiaroic behavior of the CRB can be systematically observed in the dawn and dusk sectors. Using multiple samplings of the boundary from the Defense Meteorological Satellite Program (DMSP) with time separations between each sampling from a few minutes to 25 min, we are able to resolve the CRB motion over timescales longer than 15 min. We then compare the inferred radial boundary speed with the simultaneously observed average radial speed of the plasma observed at the CRB during the course of the event. We find that 55% of the cases near dawn (06 ± 2 hr) and dusk (18 ± 2 hr) the CRB behave as an adiaroic line, but there exist significant departures from the expectation that the plasma and the boundary should move together. We conclude that the boundary motions occur on timescales much shorter than the typical 15 min duration that is accessible from this data set.

2. Data

Data from the DMSP F13, F15, F16, F17, and F18 satellites are used in this study. Each satellite orbits the Earth with a Sun-synchronous 98° inclination near 840 km altitude. A retarding potential analyzer and an ion drift meter on each spacecraft provide a measure of the velocity vector of the plasma every 4 s (F13 and F15) or every 1 s (F16, F17, and F18) with a spatial resolution of about 30 km (F13 and F15) or 7.5 km (F16, F17, and F18). The satellite orbital period of about 100 min provides 14–15 orbits a day. The average locations in magnetic local times (MLT) of each satellite when they cross 60° magnetic latitude (MLAT) on both the dawn and dusk sides in both hemispheres from 2007 to 2015 are shown in Figure 1. The time period covers only local summer seasons, May to August in the Northern Hemisphere and November to February in the Southern Hemisphere. Under these conditions, the O^+ plasma density is high and a high fidelity signal is returned from the thermal plasma sensors. The offset between the geographic and geomagnetic poles make the satellites orbits span about 2–6 hr in MLT. This allows three or four satellites to cross the north or south polar regions consecutively within 50 min at nearly the same MLT. Since some satellite orbits move in MLT in later years, there are fewer opportunities for satellite consecutive crossings near the same local time region at high latitudes.

The 1 min average IMF measurements from ACE, IMP-8, and Wind are used in this study and are available via the Space Physics Data Facility OMNIWeb interface. The IMF data are shifted by 10 min to account for propagation from the Earth's bow shock to the high-latitude ionosphere (Hairston & Heelis, 1995; Ridley et al., 1998; Yu & Ridley, 2009).

3. Approach

To investigate the plasma motion with respect to the CRB motion, we utilize both the cross-track drift velocity and the along-track drift velocity. The cross-track drift velocity is the component perpendicular to the satellite track and the along-track drift velocity is the component parallel to the satellite track. To minimize any offset in the cross-track and along-track drift velocity between each satellite due to different measurement configurations, we set the along-track drift velocity and cross-track drift velocity to zero at 50° MLAT on both duskside and dawnside of each pass and adjust the baseline linearly in time between the two locations (Archer et al., 2015; Fiori et al., 2016; Goodwin et al., 2015; Hairston & Heelis, 1990, 1995; Rich & Hairston, 1994; Weimer, 1995). We then apply a boxcar average to the cross-track and along-track drift velocity to remove

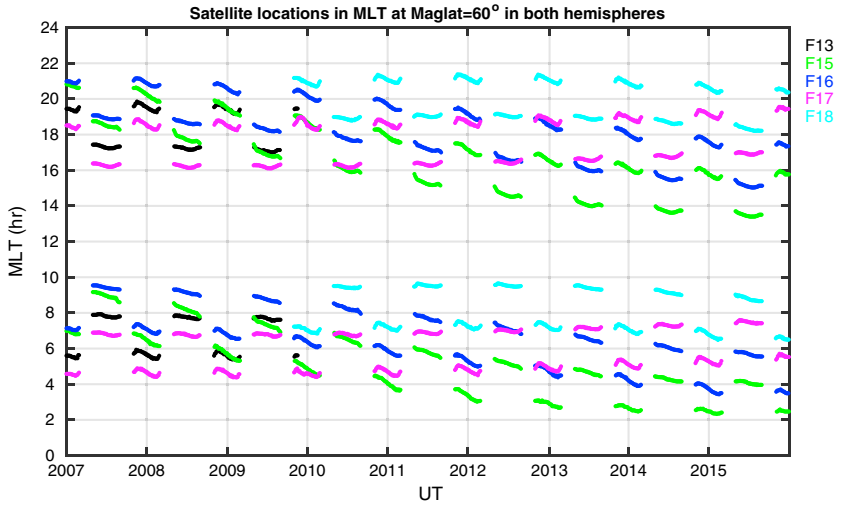

Figure 1. The location of DMSP satellite F13 (black), F15 (green), F16 (blue), F17 (magenta), and F18 (cyan) in magnetic local time (MLT) as they cross 60° in magnetic latitude during local summer seasons in both hemispheres.

structures with scale size less than 350 km (~3° in latitude) (Chen et al., 2015) and 110 km (~1° in latitude) (Chen et al., 2016), respectively for each pass, to produce a filtered data set.

By examining the filtered cross-track drift velocity data, we identify the convection reversal boundary on a pass-by-pass basis in both hemispheres. The CRB is identified as the most poleward convection reversal that separates a region of sunward flow (positive cross-track drift velocity) from a region of antisunward flow (negative cross-track drift velocity). The passes of any three satellites that cross the CRB consecutively within 50 min in universal time (UT) are collected. To ensure the satellites cross the CRB at nearly the same local time, cases where the local time span is larger than 1 hr in MLT are eliminated from this study. Changes in the latitude of the CRB are also required to be monotonically increasing or decreasing over more than 1°. This allows us to estimate an average speed of the CRB from the latitudinal changes in CRB location and the time interval between the first and third satellite crossing of the CRB.

To study the latitudinal CRB motion and the plasma flow associated with it, the horizontal flow vector for each pass (filtered along-track and cross-track drift velocity) is further resolved into radial and azimuthal components in magnetic coordinate. Then a 2° window centered at each CRB is applied to the radial flow component to determine a median value for the radial plasma flow across each CRB. The median radial flow velocity from all three satellites (V_{r1}, V_{r2}, and V_{r3}) is used to determine the average plasma motion for each event, which is compared to the radial CRB velocity determined from the latitudinal displacement of the CRB.

Figure 2 provides an example of a qualified event on 11 December 2008 taken across the dawnside CRB in the Southern Hemisphere. Cross-track drift velocity (V_y), along-track drift velocity (V_x), and radial drift velocity (V_r) (from top to bottom in the left bottom panel) are plotted as a function of MLAT for F15, F17, and F13, indicated by the color legend at the top right of the panel. The different color vertical dashed lines indicate the locations of the CRB encountered by each satellite. The trajectories of each satellite orbit as it traverses the high-latitude region from dawn to dusk are shown on the right. F15 crosses the CRB at 12:38:23 UT, which is located at (MLAT, MLT) = (−73.8°, 7.0 hr). F17 then encounters the CRB at (MLAT, MLT) = (−75.6°, 6.8 hr) about 18 min later and after another 10 min F13 crosses the CRB at (MLAT, MLT) = (−76.1°, 7.3 hr). The CRB moves continuously toward the pole about 2.3° in latitude (larger than 1°) over the time duration of about 28 min (less than 50 min), and all CRBs are encountered within 0.5 hr (less than 1 hr) in MLT. Then, a poleward speed of the net CRB motion can be simply derived as

$$V_{CRB} = \frac{-2.3\times 125,000\left(\frac{m}{\deg}\right)}{28(\min)\times 60(s)} \cong -170\left(^{m}/_{s}\right)$$

This inferred latitudinal CRB motion can be compared to the average observed radial plasma velocity at each of the CRB locations. The radial ion drift velocity from F15, F17, and F13 at the CRB is about

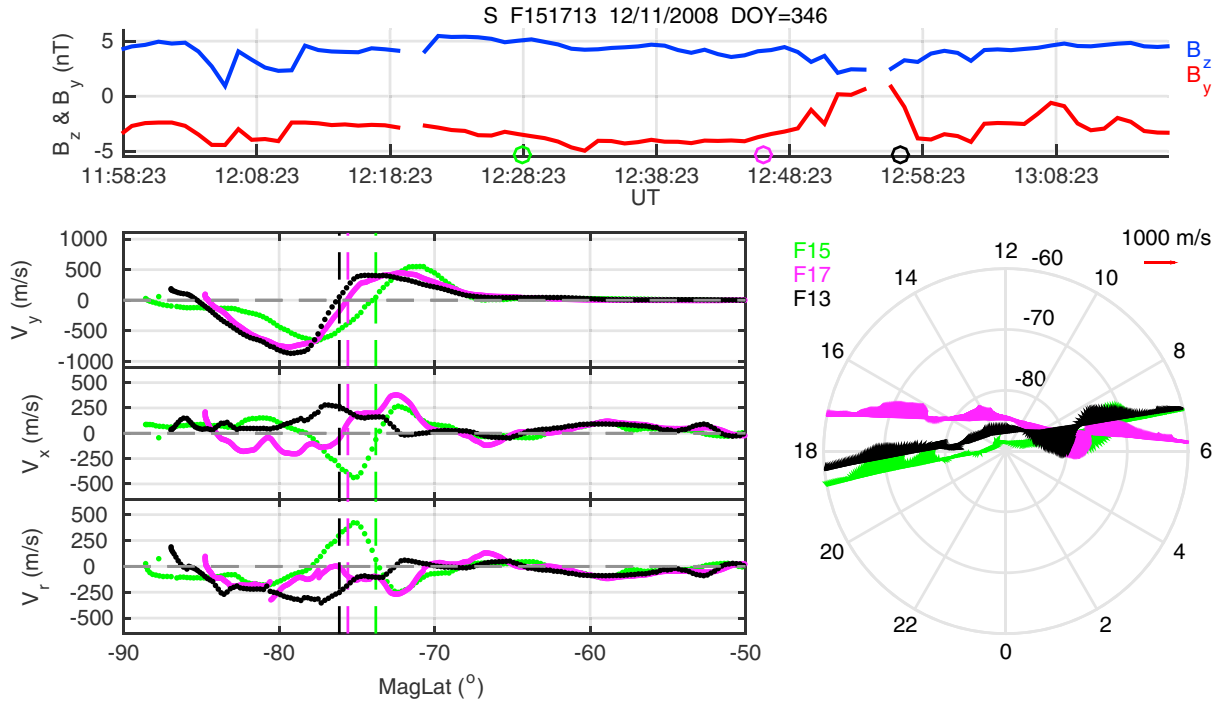

Figure 2. Sequential passes across the dawnside convection reversal boundary (CRB) in the Southern Hemisphere on 11 December 2008. Top panel shows the interplanetary magnetic field B_y and B_z in red and blue, respectively. Circles mark the time 10 min prior to the CRB crossings. In the left bottom panel, cross-track drift velocity (top), along-track drift velocity (middle), and radial plasma flow velocity (bottom) are shown with the locations of the CRBs (dashed vertical lines). The right polar diagram shows the satellite trajectories of F17, F15, and F13 across the high-latitude region from dawn to dusk in magnetic coordinate. DOY = day of year.

65 m/s directed toward the equator, 95 m/s and 250 m/s directed toward the pole. The poleward average plasma flow of 93 m/s is in the same direction as the CRB motion. The presence of radial flows due to viscous-like interaction and uncertainties in the measured plasma velocity are present and will be discussed later, but in this case a comparison of the boundary motion and the plasma motion suggests a consistency with the presence of an adiaroic boundary. 1-min average IMF B_y and B_z plotted as a function of UT in red and blue, respectively, are shown in the top panel of Figure 2. Colored circles mark the time 10 min prior to the boundary crossings of each satellite. From the IMF data we may deduce that the CRB motion is associated with the changes in IMF B_y from negative to positive as the IMF B_z changes in magnitude with a positive sign.

Several studies have shown that the CRB may not be well represented by a circle (Bristow & Spaleta, 2013; Chen et al., 2015; Koustov & Fiori, 2016). Thus, an apparent CRB motion may arise from consecutive samples displaced in local time across a CRB that is tilted with respect to a line of constant latitude. The direction and magnitude of this apparent motion will depend on the local time span between the crossings and the orientation of the CRB. Our earlier work (Chen et al., 2015) described the basic configuration of the CRB and its dependence on the IMF. As an appendix to this work we have improved a description of the shape of the CRB, which is included in the derived speed of the boundary. The apparent motion due to the tilt of the CRB will change the direction of the CRB motion only if the shape of the CRB strongly deviates from the elliptical shape shown in Appendix A. A comparison of the radial plasma flows and the inferred boundary motions for all events is presented in the following section.

4. Results and Discussions

To conduct a systematic study of the CRB motion and plasma motion associated with it, we accumulate 14,435 events with 3 boundary crossings consecutively within 50 min during local summer seasons in both hemispheres from 2007 to 2015. After applying the restriction in the latitudinal CRB displacement and the local time span of three satellites described in the previous section, we have a total of 249 events, among which 57 events show that the CRB moves continuously toward the pole or toward the equator.

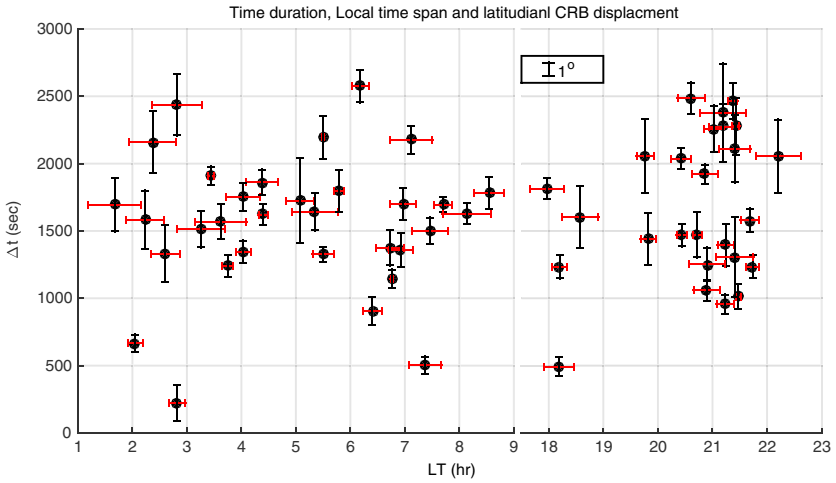

Figure 3. The local time and time duration distribution of the 57 selected events. Vertical bars and horizontal bars indicate the convection reversal boundary (CRB) displacement in latitudes and the local time span of each event, respectively.

Figure 3 summarizes the time duration and the local time distribution of the 57 selected events with the vertical and horizontal bars indicating the latitudinal CRB displacement and the local time span of the CRB detected by the three satellites, respectively. The events are distributed more evenly in the dawn sector between 2 and 9 hr than in the local time sector on the duskside. There are no events located between 9 and 17 hr and only a few events in the prenoon sector. This is due to the fact that about 95% of the qualified events are taken in the Southern Hemisphere where the satellites seldom transverse the region between local noon and dusk. Most of the cases have time durations between 15 and 40 min, which allows us to investigate the dynamics of the CRB on timescales of tens of minutes. The latitudinal displacement of the CRB varies from 1° to 7°, which means the speed of the CRB varies significantly.

Following the procedure described in the previous section, we compared the average radial flow velocity across the CRB measured by the three satellite ($<V_r>$) in each sequential event to the estimated velocity of the CRB from the changes in the CRB location and the time interval between the first and third crossings. The results are shown in Figure 4 with dawnside crossings on the right and duskside crossings on the left. The colors indicate the CRB location in MLT recognized by the second satellite. The error bar indicates the variability in the radial velocity from the three satellites. A positive velocity means the plasma flow or the CRB motion is directed toward the equator and a negative velocity means the plasma flow or the CRB motion is directed toward the pole. We find 70% of all events show agreement in the inferred and measured direction of the CRB motion (first and third quadrants), while 30% show disagreement in the direction (second and fourth quadrants).

There are intrinsic uncertainties in the derivation of the flow velocity itself and in identifying the location of the CRB that is used to infer the boundary motion. When we use the filtered cross-track drift velocity to identify the CRB location the uncertainty in the location of the CRB can be introduced and could be large if the flow around the CRB is structured. Most of the cases with the structure around the CRB that could affect the inferred CRB motion are located closer to local noon and midnight or have longer duration between three observations. This can also affect the plasma flow velocity across the CRB used to compare with the CRB motion. We conservatively estimate an uncertainty of 100 m/s from these sources (Chen et al., 2016) and provide an estimated envelope (dashed straight lines) within which the observed boundary motion and the measured plasma motion are consistent with the presence of an adiaroic boundary. There are 10 events in the dusk sector and 15 events in the dawn sector, which is ~45% of all events, falling within this dashed line region. The points outside these envelopes have a larger deviation between the CRB motion and plasma motion than can be expected for the uniform motion of an adiaroic boundary over the time period considered.

Our data selection procedure does not remove samples of the CRB that are close to local noon and local midnight. Thus, it is possible to sample a region where active reconnection is taking place. In such

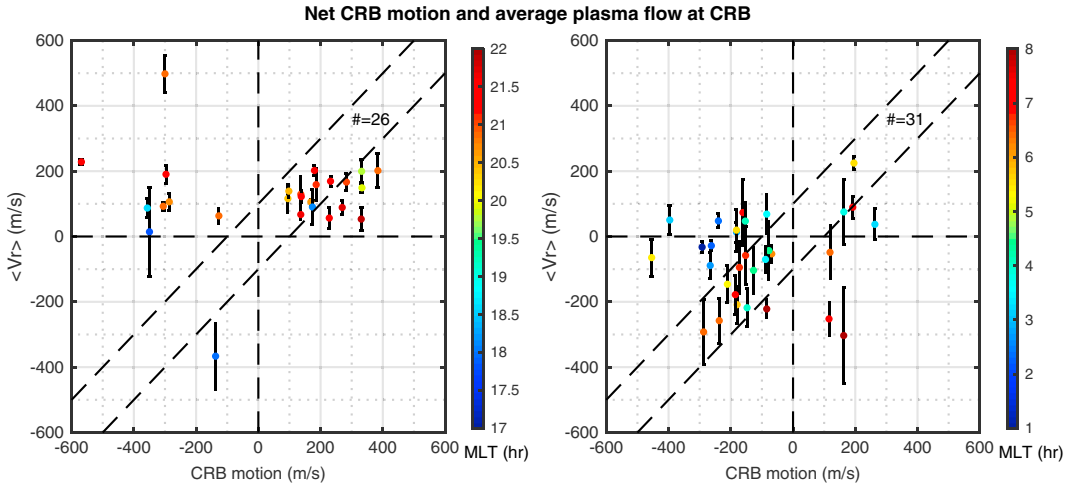

Figure 4. Average radial plasma flow from the three satellites and estimated speed of the convection reversal boundary (CRB) motion are plotted against each other in the scatter diagrams. The colors represent the CRB location in magnetic local time (MLT). Dashed lines indicate the area within which the CRB motion and the plasma motion are consistent with the presence of an adiaroic boundary.

circumstances we may expect that the inferred boundary motions and the measured plasma flows will be oppositely directed with large measured flows. However, in our 57 events, no samples are taken near local noon where active reconnection sites are expected. To minimize the influence from nightside reconnection, the local time region can be restricted to near the dawn (06 ± 2 hr) and dusk (18 ± 2 hr) where the boundary is most likely to be an adiaroic line. Then, there remain 10 events among a total of 23, which is about 45% of cases outside the dashed line that bounds our consistency envelope.

A difference in the inferred boundary motion and the plasma motion may arise from the presence of a viscous-like interaction across a boundary, which would otherwise expand and contract with the plasma flow. Previous studies (Chen et al., 2016, and references therein) have shown that viscous-like flows of up to 100 m/s across the CRB may be present. This allows the inferred boundary motion and measured plasma flows to differ in magnitude and, when the measured flows are small, in direction. A few points that have positive radial velocities in the premidnight and postmidnight local time region may be brought to the envelope of consistency by accounting for the presence of viscous-like flows. Then, about 60% of events near dawn and dusk fall within the consistency envelope. While it is possible to arbitrarily move points along the *y* axis by up to 100 m/s to place them within the envelope of consistency, there is no systematic correction in the flows that can be made since the dependence of the magnitude and direction of viscous-like flows on local time is unknown.

We conclude that 45% of the events in local time region near dawn (06 ± 2 hr) and dusk (18 ± 2 hr) show large deviation between the CRB motion and plasma motion, which are inconsistent with the monotonic motion of an adiaroic boundary over the observed timescale. If we invoke the presence of flows from viscous interaction there remain 40% of cases that cannot be reconciled with the monotonic motion of an adiaroic boundary.

Finally, we note that our comparison of inferred boundary motions and plasma flows is based on sequential crossings of the CRB that are spaced in time over several tens of minutes. If the boundary advances monotonically over a period corresponding to the time between sequential samples but also moves back and forth on a timescale shorter than the typical sample time, then the measured flow velocity for any sample may differ in magnitude and direction from that inferred by the sequential samples around it. Most of the events for which the inferred boundary motions are inconsistent with measured plasma flows require this hypothesis to be consistent with an adiaroic boundary. We also examined the variations in the IMF B_y and B_z between the three crossings case by case. For 20% of the events, the IMF B_y or B_z shows large variation (more than 2 nT) between sequential samplings of the CRB. About half of the events (five events) with this large variation show inconsistent CRB motion and plasma motion. This variation together with the sample spacing in time could affect the comparison of inferred CRB motion and plasma motion. Figures 5 and 6 are examples that illustrate the short-timescale CRB motion and the variations in the IMF.

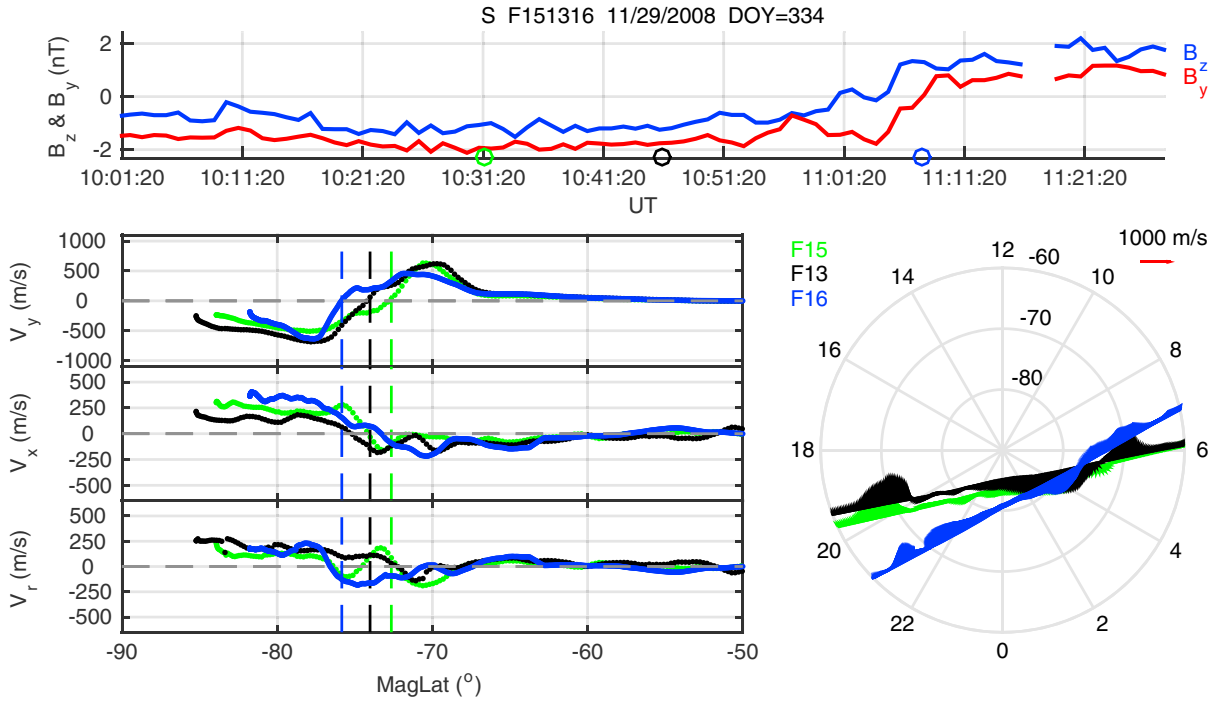

Figure 5. Sequential passes across the dawnside convection reversal boundary in the Southern Hemisphere on 29 November 2008. The format is same as Figure 2. DOY = day of year.

On 29 November 2008 in the Southern Hemisphere (Figure 5) F15, F13, and F16 encounter the CRB at 10:41:20 UT, 10:56:09 UT, and 11:17:55 UT with the corresponding CRB location at (MLAT, MLT) = (−72.6°, 5.47 hr), (MLAT, MLT) = (−74°, 5.51 hr), and (MLAT, MLT) = (−75.8°, 5.49 hr). The satellites cross the CRBs at the same local time thus the effect from the tilt of the CRB should be negligible. The CRB moves 3.2° poleward in latitude during 37 min which gives us an estimated poleward speed of the CRB ~180 m/s. The plasma flow measured by F15 and F13 are about 90 and 100 m/s equatorward. That is in the opposite direction of the inferred CRB motion. The third satellite, F16, observes a poleward plasma flow ~130 m/s which is in the same direction with the inferred CRB motion. We note that the motion of CRB observed by these three satellites is in accord with the changes in the both B_y and B_z from negative to slightly positive with a 1 nT variation in IMF B_y between the sequential crossings without considering a 10 min time shift in the IMF data. In this study, we used an average 10 min to account for the propagation from the bow shock to the observed region in the high-latitude ionosphere. However, this time shift could be shorter, dependent on the solar wind speed and the timing of the response of ionosphere (Ruohoniemi et al., 2002; Yu & Ridley, 2009).

At this local time near dawn we might expect any flow across the CRB due to the presence of a viscous-like interaction to be quite small. Regardless of the direction of this flow, it cannot be used to reconcile the difference between the inferred boundary motion and the measured plasma flows. In this case the most straightforward interpretation is to invoke a rapid poleward motion of the boundary and the plasma on a timescale that is short compared to the time between CRB crossings, which is on the order of 15 min. Such a poleward motion, approximately twice the observed flow speeds, occurring between the first and second boundary crossings and between the second and third boundary crossings would reconcile this and many of the cases for which the inferred boundary velocity and the measured plasma flow have the opposite sign.

Figure 6 shows an example with a rapid change in plasma motion over a short time period. F15 crosses the CRB at 12:14:47 UT which is located at (MLAT, MLT) = (−73.2°, 6.7 hr). F17 then encounters the CRB at (MLAT, MLT) = (−74.4°, 6.4 hr) about 4 min later and after another 19 min F13 crosses the CRB at (MLAT, MLT) = (−75.9°, 6.9 hr). The CRB moves continuously toward the pole by about 2.7° in latitude over 23 min. The inferred CRB speed is about 245 m/s. The radial ion drift velocity from F15, F17, and F13 at the CRB is about 260 m/s, 390 m/s, and 120 m/s directed toward the pole. While the average plasma flow over these three measurements is about 255 m/s, which is comparable to the inferred CRB motion, the plasma velocity sampled

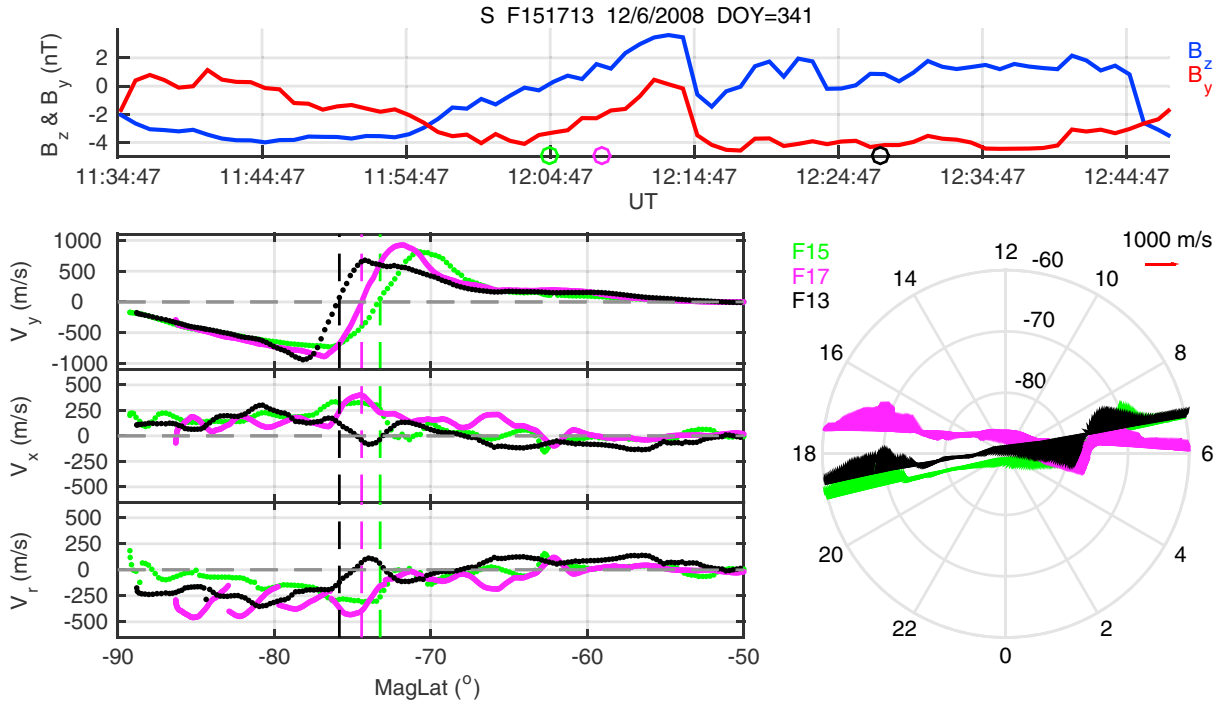

Figure 6. Sequential passes across the dawnside convection reversal boundary in the southern hemisphere on 6 December 2008. The format is same as Figure 2. DOY = day of year.

by the second satellite exceeds the inferred boundary velocity by about 150 m/s. The IMF B_y and B_z both vary by more than 2 nT during the event which is associated with the rapid changes in plasma flow. We also note that the measured plasma flow changes about 130 m/s in the first 4 min. This rapid change along with the average measured flow speed that is comparable with inferred CRB speed further supports the hypothesis that the CRB and plasma move radially with velocities on the order of 100 m/s on timescales of a few minutes.

5. Summary

A systematic study of the convection reversal boundary motion and the plasma motion across it was conducted by analyzing multiple samplings of the CRB from the DMSP with time separations between each satellite from a few minutes to 25 min. Using this data set, we are able to examine the behavior of the adiaroic CRB in the dawn and dusk sectors on a timescale longer than 15 min. After considering the intrinsic uncertainty in the flow measurements and boundary identification, we find that ~55% of the time the CRB motion largely deviates from the local plasma. In the local time region near dawn and dusk, there remain 45% of the cases that show large deviation between the CRB and plasma motion. If the CRB must present the property of an adiaroic boundary then the difference between the inferred CRB speed and the flow speed can arise in several scenarios.

First, an apparent CRB motion, which is produced by the sequential samplings in local time of a CRB that is tilted with respect to a constant latitude line, can contribute to the differences in the CRB and plasma motion. We note that the distortion of the boundary will need to be severe in order to remain after a nominal correction for the usually observed shape. It thus seems unlikely that deviations from a quasi-steady adiaroic behavior near dawn and dusk may be attributed to this phenomenon. Viscous-like interaction allows inferred boundary motion and measured plasma flows to differ in magnitude and in direction depending on local time and the magnitude of the measured flow. We have previously mentioned that some observations may be brought into compliance with the expectations for a monotonic motion of an adiaroic boundary by invoking the presence of such flows, but there remain at least 40% of cases near dawn and dusk that cannot be accommodated in this way. Thus, 40% of the observations are inconsistent with monotonic motion of an adiaroic line over the timescales considered. The most straightforward explanation for this behavior is an expectation that the CRB may move back and forth on timescales of a few minutes in addition to a poleward

or equatorward motion over longer timescales. This hypothesis that the CRB has both a long-timescale (>15 min) motion and a short-timescale (<15 min) jitter that are comparable in magnitude can reconcile most of the events for which the inferred boundary motions and the measured plasma flows disagree.

Appendix A: Configuration of the Convection Reversal Boundary

Data are taken from F13, F15, F16, F17, and F18 during the local summer seasons from 2000 to 2015. The same procedure used in Chen et al. (2015) is applied to this larger database to identify the location of the convection reversal boundary for different orientations and magnitudes of the IMF. This larger database improves the local time coverage describing the boundary location and produces a more complete and higher-resolution description of the CRB configuration.

Figure A1 shows the location of the boundaries in both hemispheres under weakly southward IMF conditions (top) and strongly southward IMF conditions (bottom) with different polarities in B_y. The red, green, pink, blue, and black dotted solid lines indicate the location of the boundaries corresponding respectively to the ranges of IMF B_y: $B_y \geq 3.3$, $1 \leq B_y < 3.3$, $-1 \leq B_y < 1$, $-3.3 \leq B_y < -1$, and $B_y \leq -3.3$. We mark the local time bin with a hollowed circle where the number of samples is extremely low (less than 5). As expected most of the hollowed circles are at local time later than 20 h and earlier than 3 h in the Northern Hemisphere (left panels) and local noon in the southern hemisphere (right bottom panel) where the satellites seldom pass.

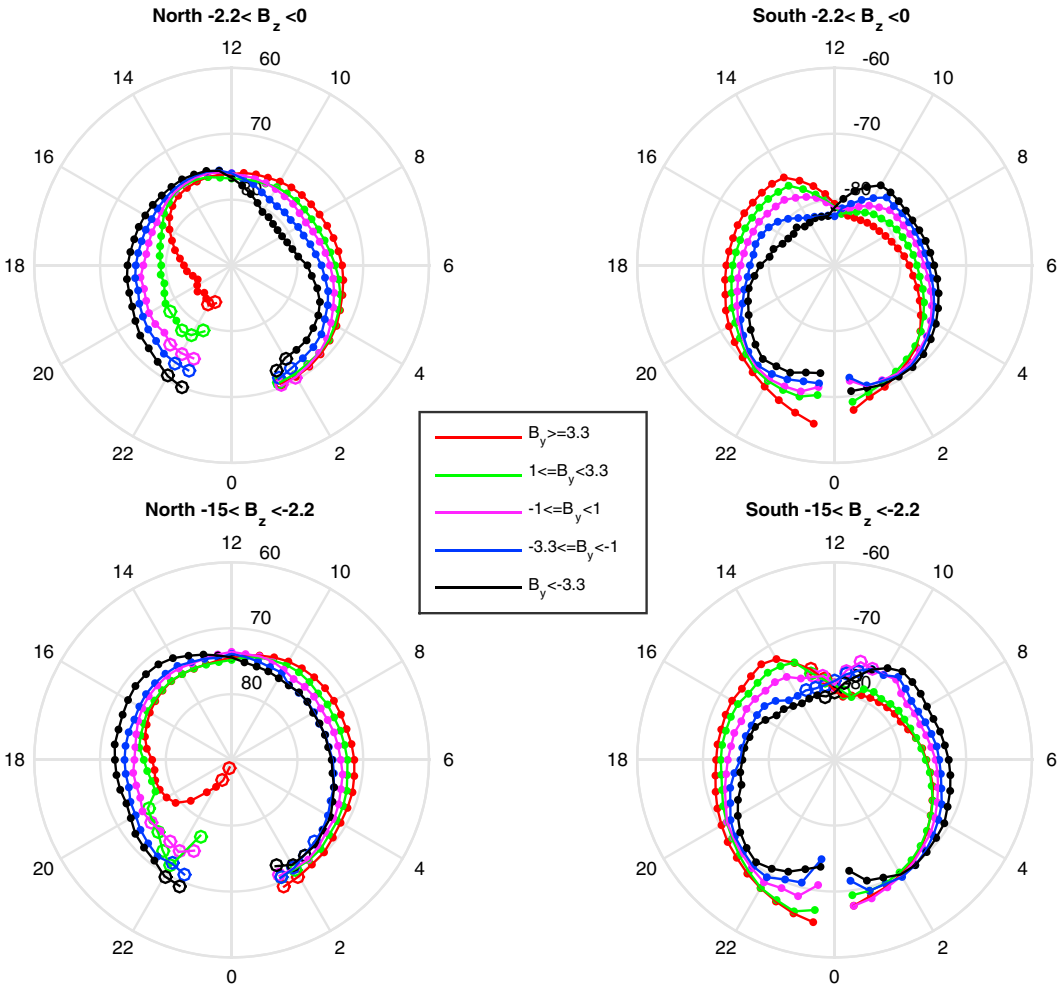

Figure A1. Convection reversal boundary locations in the Northern Hemisphere (left) and Southern Hemisphere (right) for weakly southward B_z (top) and strongly southward B_z (bottom).

At the dayside reconnection region, a latitudinal offset between the prenoon and postnoon boundary results in a gap opened toward dawn/dusk for positive/negative B_y in the Southern Hemisphere. The opposite dependencies on B_y are seen in the Northern Hemisphere. We note that in the Northern Hemisphere when IMF B_z is strongly southward, this latitudinal asymmetry between the dawnside and duskside boundaries appear here as expected but is not seen using the more limited data set in Chen et al. (2015). Across midnight this latitudinal offset is not so apparent and thus may not have a dependency on B_y as seen on the dayside. The CRB representations suggested by Chen et al. (2015) show ellipses that have co-aligned semimajor axes but different lengths that allow a latitudinal displacement of a dayside gap in the boundary with the boundary being more continuous across midnight. This more accurate description of the CRB shape allows a correction for the effective motion of the boundary that would result from consecutive samples of the boundary that are displaced in local time.

Acknowledgments
This work is supported by NASA grant NNX14AF33G to the University of Texas at Dallas and by AFOSR MURI grant FA9559-16-1-0364. The interplanetary magnetic field data are available via the Space Physics Data Facility OMNIWeb interface. The link to this database is http://omniweb.gsfc.nasa.gov. The DMSP ion drift data were obtained from the William B. Hanson Center for Space Sciences at the University of Texas at Dallas. The data before 2005 are available at http://cindispace.utdallas.edu/DMSP/dmsp_data_at_utdallas.html, and the data after 2005 can be requested from Marc Hairston (hairston@utdallas.edu). The authors thank Robin Coley, Marc Hairston, and Bob Power for its use.

References

Archer, W. E., Knudsen, D. J., Burchill, J. K., Patrick, M. R., & St.-Maurice, J. P. (2015). Anisotropic core ion temperatures associated with strong zonal flows and upflows. *Geophysical Research Letters*, *42*, 981–986. https://doi.org/10.1002/2014GL062695

Axford, W. I. (1964). Viscous interaction between the solar wind and the Earth's magnetosphere. *Planetary and Space Science*, *12*(1), 45–53. https://doi.org/10.1016/0032-0633(64)90067-4

Axford, W. I., & Hines, C. O. (1961). A unifying theory of high latitude geophysical phenomena and magnetic storms. *Canadian Journal of Physics*, *39*(10), 1433–1464. https://doi.org/10.1139/p61-172

Boyle, C. B., Reiff, P. H., & Hairston, M. R. (1997). Empirical polar cap potentials. *Journal of Geophysical Research*, *102*(A1), 111–125. https://doi.org/10.1029/96JA01742

Bristow, W. A., & Spaleta, J. (2013). An investigation of the characteristics of the convection reversal boundary under southward interplanetary magnetic field. *Journal of Geophysical Research: Space Physics*, *118*, 6338–6351. https://doi.org/10.1002/jgra.50526

Brittnacher, M., Fillingim, M., Parks, G., Germany, G., & Spann, J. (1999). Polar cap area and boundary motion during substorms. *Journal of Geophysical Research*, *104*(A6), 12,251–12,262. https://doi.org/10.1029/1998JA900097

Chen, Y.-J., Heelis, R. A., & Cumnock, J. A. (2015). Response of the ionospheric convection reversal boundary at high latitudes to changes in the interplanetary magnetic field. *Journal of Geophysical Research: Space Physics*, *120*, 5022–5034. https://doi.org/10.1002/2015JA021024

Chen, Y.-J., Heelis, R. A., & Cumnock, J. A. (2016). Plasma and convection reversal boundary motions in the high-latitude ionosphere. *Journal of Geophysical Research: Space Physics*, *121*, 5752–5763. https://doi.org/10.1002/2016JA022796

Cousins, E. D. P., & Shepherd, S. G. (2010). A dynamical model of high-latitude convection derived from SuperDARN plasma drift measurements. *Journal of Geophysical Research*, *115*, A12329. https://doi.org/10.1029/2010JA016017

Cowley, S. W. H., & Lockwood, M. (1992). Excitation and decay of solar wind-driven flows in the magnetosphere-ionosphere system. *Annales Geophysique*, *10*, 103–115.

Drake, K. A., Heelis, R. A., Hairston, M. R., & Anderson, P. C. (2009). Electrostatic potential drop across the ionospheric signature of the low-latitude boundary layer. *Journal of Geophysical Research*, *114*, A04215. https://doi.org/10.1029/2008JA013608

Dungey, J. W. (1961). Interplanetary magnetic field and the auroral zones. *Physical Review Letters*, *6*(2), 47–48. https://doi.org/10.1103/PhysRevLett.6.47

Fiori, R. A. D., Boteler, D. H., & Koustov, A. V. (2012). Response of ionospheric convection to sharp southward IMF turnings inferred from magnetometer and radar data. *Journal of Geophysical Research*, *117*, A09302. https://doi.org/10.1029/2012JA017755

Fiori, R. A. D., Kouston, A. V., Boteler, D. H., Knudsen, D. J., & Burchill, J. K. (2016). Calibration and assessment of Swarm ion drift measurements using a comparison with a statistical convection model. *Earth, Planets and Space*, *68*(1), 1–17. https://doi.org/10.1186/s40623-016-0472-7

Gjerloev, J. W., Hoffman, R. A., Sigwarth, J. B., Frank, L. A., & Baker, J. B. H. (2008). Typical auroral substorm: Abifurcated oval. *Journal of Geophysical Research*, *113*, A03211. https://doi.org/10.1029/2007JA012431

Goodwin, L. V., Iserhienrhien, B., Miles, D. M., Patra, S., van der Meeren, C., Buchert, S. C., et al. (2015). Swarm in situ observations of F region polar cap patches created by cusp precipitation. *Geophysical Research Letters*, *42*, 996–1003. https://doi.org/10.1002/2014GL062610

Hairston, M. R., & Heelis, R. A. (1990). Model of the high-latitude ionospheric convection pattern during southward interplanetary magnetic field using DE 2 data. *Journal of Geophysical Research*, *95*(A3), 2333–2343. https://doi.org/10.1029/JA095iA03p02333

Hairston, M. R., & Heelis, R. A. (1995). Response time of the polar ionospheric convection pattern to changes in the north-south direction of the IMF. *Geophysical Research Letters*, *22*(5), 631–634. https://doi.org/10.1029/94GL03385

Heelis, R. A. (1984). The effects of interplanetary magnetic field orientation on dayside high-latitude ionospheric convection. *Journal of Geophysical Research*, *89*(A5), 2873–2880. https://doi.org/10.1029/JA089iA05p02873

Koustov, A. V., & Fiori, R. A. D. (2016). Seasonal and solar cycle variations in the ionospheric convection reversal boundary location inferred from monthly SuperDARN data sets. *Annales Geophysique*, *34*(2), 227–239. https://doi.org/10.5194/angeo-34-227-2016

Laundal, K. M., Østgaard, N., Frey, H. U., & Weygand, J. M. (2010). Seasonal and interplanetary magnetic field–dependent polar cap contraction during substorm expansion phase. *Journal of Geophysical Research*, *115*, A11224. https://doi.org/10.1029/2010JA015910

Lockwood, M., Hairston, M., Finch, I., & Rouillard, A. (2009). Transpolar voltage and polar cap flux during the substorm cycle and steady convection events. *Journal of Geophysical Research*, *114*, A01210. https://doi.org/10.1029/2008JA013697

Lockwood, M., & Morley, S. K. (2004). A numerical model of the ionospheric signatures of time varying magnetic reconnection: I. Ionospheric convection. *Annales Geophysique*, *22*(1), 73–91. https://doi.org/10.5194/angeo-22-73-2004

Morley, S. K., & Lockwood, M. (2006). A numerical model of the ionospheric signatures of time-varying magnetic reconnection: III. Quasi-instantaneous convection responses in the Cowley–Lockwood paradigm. *Annales Geophysique*, *24*(3), 961–972. https://doi.org/10.5194/angeo-24-961-2006

Moses, J. J., Siscoe, G. L., Heelis, R. A., & Winningham, J. D. (1988). A model for multiple throat structures in the polar cap flow entry region. *Journal of Geophysical Research*, *93*(A9), 9785–9790. https://doi.org/10.1029/JA093iA09p09785

Mozer, F. S. (1984). Electric field evidence on the viscous interaction at the magnetopause. *Geophysical Research Letters*, *11*(2), 135–138. https://doi.org/10.1029/GL011i002p00135

Nishitani, N., Ogawa, T., Sato, N., Yamagishi, H., Pinnock, M., Villain, J.-P., et al. (2002). A study of the dusk convection cell's response to an IMF southward turning. *Journal of Geophysical Research*, *107*(A3), 1036. https://doi.org/10.1029/2001JA900095

Rich, F. J., & Hairston, M. (1994). Large-scale convection patterns observed by DMSP. *Journal of Geophysical Research*, *99*(A3), 3827–3844. https://doi.org/10.1029/93JA03296

Ridley, A. J., & Clauer, C. R. (1996). Characterization of the dynamic variations of the dayside high-latitude ionospheric convection reversal boundary and relationship to interplanetary magnetic field orientation. *Journal of Geophysical Research*, *101*(A5), 10,919–10,938. https://doi.org/10.1029/95JA03805

Ridley, A. J., Lu, G., Clauer, C. R., & Papitashvili, V. O. (1998). A statistical study of the ionospheric convection response to changing interplanetary magnetic field conditions using the assimilative mapping of ionospheric electrodynamics technique. *Journal of Geophysical Research*, *103*(A3), 4023–4039. https://doi.org/10.1029/97JA03328

Ruohoniemi, J. M., & Greenwald, R. A. (1996). Statistical patterns of high-latitude convection obtained from Goose Bay HF radar observations. *Journal of Geophysical Research*, *101*(A10), 21,743–21,763. https://doi.org/10.1029/96JA01584

Ruohoniemi, J. M., Shepherd, S. G., & Greenwald, R. A. (2002). The response of the high-latitude ionosphere to IMF variations. *Journal of Atmospheric and Terrestrial Physics*, *64*(2), 159–171. https://doi.org/10.1016/S1364-6826(01)00081-5

Siscoe, G. L., & Huang, T. S. (1985). Polar cap inflation and deflation. *Journal of Geophysical Research*, *90*(A1), 543–547. https://doi.org/10.1029/JA090iA01p00543

Sonnerup, B. U., Siebert, K. D., White, W. W., Weimer, D. R., Maynard, N. C., Schoendorf, J. A., et al. (2001). Simulations of the magnetosphere for zero interplanetary magnetic field: The ground state. *Journal of Geophysical Research*, *106*(A12), 29,419–29,434. https://doi.org/10.1029/2001JA000124

Sundberg, K. Å. T., Blomberg, L. G., & Cumnock, J. A. (2008). Statistical analysis of the sources of the cross-polar potential for southward IMF, based on particle precipitation characteristics. *Geophysical Research Letters*, *35*, L08103. https://doi.org/10.1029/2008GL033383

Weimer, D. R. (1995). Models of high-latitude electric potentials derived with a least error fit of spherical harmonic coefficients. *Journal of Geophysical Research*, *100*(A10), 19,595–19,607. https://doi.org/10.1029/95JA01755

Weimer, D. R. (2001). An improved model of ionospheric electric potentials including substorm perturbations and application to the Geospace Environment Modeling November 24, 1996, event. *Journal of Geophysical Research*, *106*(A1), 407–416. https://doi.org/10.1029/2000JA000604

Weimer, D. R. (2005). Improved ionospheric electrodynamic models and application to calculating Joule heating rates. *Journal of Geophysical Research*, *110*, A05306. https://doi.org/10.1029/2004JA010884

Yu, Y., & Ridley, A. J. (2009). Response of the magnetosphere-ionosphere system to a sudden southward turning of interplanetary magnetic field. *Journal of Geophysical Research*, *114*, A03216. https://doi.org/10.1029/2008JA013292